

Oscillatory convection in a two-dimensional porous box with asymmetric lateral boundary conditions

D. Andrew S. Rees

Department of Mechanical Engineering, University of Bath, Claverton Down, Bath BA2 7AY, United Kingdom

Peder A. Tyvand

Department of Agricultural Engineering, Agricultural University of Norway, 1432 Ås, Norway

(Received 21 July 2003; accepted 18 June 2004; published online 1 September 2004)

The onset of convection in a two-dimensional porous cavity is investigated where the cavity is subject to asymmetric boundary conditions at the lateral walls: one vertical wall is thermally conducting and impermeable, while the other is thermally insulating and open. At the open boundary the saturating fluid flows freely in and out from a hydrostatic reservoir in contact with the porous medium. The top and bottom of the box are impermeable and perfectly conducting. It is shown that the mode for onset of convection is oscillatory in time. This corresponds to a disturbance traveling as a wave through the box from the impermeable wall to the open wall. The preferred eigensolution, its oscillation frequency, and critical Rayleigh number are calculated numerically for different aspect ratios of the porous box, and these values are confirmed by means of suitable asymptotic analyses. © 2004 American Institute of Physics. [DOI: 10.1063/1.1781160]

I. INTRODUCTION

The classical problem of the onset of convection in a porous layer heated from below is nonoscillatory.^{1,2} The Horton–Rogers–Lapwood problem assumes impermeable and perfectly conducting top and bottom planes. These conditions were generalized by Nield³ to include the cases of constant pressure and constant heat flux. Despite these altered conditions the single-diffusive onset of convection is governed by strictly nonoscillatory modes of instability.

Straus⁴ investigated the stability of finite-amplitude convection in the Horton–Rogers–Lapwood problem. The preferred modes of secondary instability in a layer of infinite horizontal extent are also nonoscillatory. This means that the first oscillations may appear at third level in a hierarchy of instabilities, which will require highly supercritical Rayleigh numbers.

In a finite box, oscillatory instability may set in somewhat earlier as a secondary instability.⁵ In a two-dimensional square box this oscillatory instability takes place at a Rayleigh number of order 10 times that of the onset of convection. Accurate computations of the triggering of oscillatory convection were performed by Aidun and Steen⁶ and Kimura, Schubert, and Straus.⁷ Kimura, Schubert, and Straus⁸ investigated three-dimensional oscillatory convection in a cube. They found oscillations as a secondary instability occurring at a Rayleigh number somewhat higher than that of two-dimensional flow. In these papers, the lateral walls are taken as thermally insulating.

Oscillatory convection in the presence of a single-diffusive component is acknowledged as a nonlinear phenomenon, appearing at Rayleigh numbers one order of magnitude above the threshold for onset. One would not expect oscillations to take place in a linearized Horton–Rogers–Lapwood problem for a finite box.

A first analysis of the linear theory for a finite porous box was performed by Wooding,⁹ who considered the asymptotic limit of tall porous cylinders. His results were complemented by exact results for the rectangular box derived by Beck¹⁰ and the circular cylinder derived by Zebib.¹¹ Again no oscillations were found, but this was physically reasonable because of the traditional boundary conditions applied at the lateral walls. These wall conditions are identical to those which are valid at the internal cell walls, and correspond to the wall being impermeable and thermally insulating. The above-mentioned studies of finite porous boxes can, in general, be constructed from superposing modes of convection for an porous layer of infinite extent, once we specify the appropriate wave numbers which fit in with the geometry.

The physics changes somewhat when the conditions applied at the lateral wall of a finite box are nontraditional. Nontraditional wall conditions are those which do not correspond to the conditions at internal cell walls. Yet one would expect only quantitative changes to take place when nontraditional lateral conditions are introduced. However, the present paper shows that it is possible to introduce oscillations at the onset of convection by means of asymmetric nontraditional lateral conditions.

The first exact analysis of the onset of convection in a box with nontraditional lateral conditions was performed by Nilsen and Storesletten.¹² They assumed impermeable and conducting lateral walls, and their analysis was confirmed by Rees and Lage.¹³ Since both lateral walls were identical, the onset mode could be given as a superposition of one symmetric mode and one antisymmetric mode with respect to the middle of the box. These symmetries do not allow traveling waves to occur.

The condition of an impermeable and conducting wall can be called the first nontraditional wall condition. There is

a second nontraditional wall condition: the case where the wall is hydrostatic (free horizontal throughflow of the saturating fluid) and thermally insulating. By considering the first nontraditional condition valid at the left-hand wall in combination with the second nontraditional condition valid at the right-hand wall, we obtain a configuration without left/right symmetry. The left-hand boundary allows heat transfer without mass transfer. The right-hand boundary allows mass transfer without heat transfer. This type of physical antisymmetry implies no mathematical symmetry, and it induces a wave traveling from left to right at the onset of convection, as will be shown by the analysis below. These nontraditional boundary conditions do not allow the mathematical solution to be extended outside the porous box. This is in contrast to the traditional conditions corresponding to cell walls, where a symmetric extension outside a boundary describes a possible neighboring cell in a larger cavity.

The present physical problem gives an astonishingly simple mechanism of generating oscillations in a porous medium. We believe that it is the simplest possibility available for oscillatory convection in a porous medium. It is a simpler mechanism for oscillations than the standard one, which was first identified by Horne and O’Sullivan.⁵

II. BASIC EQUATIONS

We consider a two-dimensional porous medium with a homogeneous and isotropic permeability K . Cartesian coordinates x, y are introduced, where the y axis points vertically upwards. The porous medium occupies a rectangular box with length L in the x direction and height H in the y direction.

The temperature field is $T(x, y, t)$, where t denotes time. There is an undisturbed state of pure conduction where the lower plane $y=0$ is kept at a constant temperature $T_0 + \Delta T$ and the upper plane $y=H$ is kept at a constant temperature T_0 . We will perturb this state of pure conduction, but the temperatures at the top and bottom surfaces are kept constant. This means that the perturbation temperature $\theta(x, y, t)$ is assumed to vanish at the top and bottom of the porous box. The top and bottom surfaces are assumed to be impermeable.

We choose the following units for dimensionless time, velocity, and pressure:

$$(c_p \rho)_m H^2 / k_m, \quad \kappa_m / H, \quad \rho_0 \nu \kappa_m / K, \tag{1}$$

respectively, where c_p is the specific heat at constant pressure, k is the heat conductivity, κ is the thermal diffusivity, ν is the kinematic viscosity of the saturating fluid, and ρ_0 is a reference fluid density. The subscript m represents the mixture of solid and fluid, and the subscript f will represent the saturating fluid.

Our dimensionless Darcy–Boussinesq equations for convection in a homogeneous and isotropic porous medium are given by

$$\underline{v} + \nabla p - \text{Ra} T \underline{j} = 0, \tag{2}$$

$$\nabla \cdot \underline{v} = 0, \tag{3}$$

$$\frac{\partial T}{\partial t} + \underline{v} \cdot \nabla T = \nabla^2 T. \tag{4}$$

The Rayleigh number for a porous medium is given by

$$\text{Ra} = \frac{g \beta K \Delta T H}{\nu \alpha_m}. \tag{5}$$

We have introduced g as the gravitational acceleration and β as the expansion coefficient. In Eqs. (2)–(4), \underline{v} is the velocity, while p is the pressure, and \underline{j} is the vertical unit vector. The basic dimensionless temperature gradient is -1 and is due to pure conduction. We perturb the basic temperature field and introduce the temperature perturbation $\theta(x, y, t)$ as follows:

$$T = 1 - y + \theta(x, y, t). \tag{6}$$

We introduce the stream function ψ and eliminate the pressure. The governing equations are

$$\nabla^2 \psi - R \frac{\partial \theta}{\partial x} = 0, \tag{7}$$

$$\nabla^2 \theta + \frac{\partial \psi}{\partial x} = \frac{\partial \theta}{\partial t}. \tag{8}$$

The velocity components are $(u, v) = (-\partial \psi / \partial y, \partial \psi / \partial x)$.

As boundary conditions in the vertical direction we take the standard conditions of impermeable and conducting top and bottom planes:

$$\psi = \theta = 0 \quad \text{at} \quad y = 0, \quad y = 1. \tag{9}$$

These are the conditions that are applied in the classical Horton–Rogers–Lapwood problem. The lateral wall conditions are nontraditional, however. At the left-hand end we assume an impermeable and conducting wall:

$$\psi = \theta = 0 \quad \text{at} \quad x = 0. \tag{10}$$

Physically this means that the wall is a much better heat conductor than the saturated porous medium. Still the heat conductivity of the wall must be considerably smaller than that of the top and bottom planes.

We assume the right-hand end of the porous rectangle to be thermally insulating and open:

$$\frac{\partial \psi}{\partial x} = \frac{\partial \theta}{\partial x} = 0 \quad \text{at} \quad x = a. \tag{11}$$

An open boundary means that the porous medium is in contact with a neighboring hydrostatic reservoir where the saturating fluid can flow freely in and out.

Our aim in introducing the thermal boundary condition in (11) is primarily mathematical, for the nontraditional boundary conditions given in (10) give rise to degeneracy at onset when they apply to both sidewalls; the proof of degeneracy given by Rees and Tyvand¹⁴ relies on the boundary conditions for ψ and θ being identical. Therefore we have used identical boundary conditions for ψ and θ in (11) for the right-hand sidewall. Intuitively it seems contradictory that a boundary can be open to mass flux and closed to heat flux. So let us demonstrate how these conditions (11) arise as limit cases of the general conditions valid at the boundary between

two porous media, according to linear theory. We consider one porous medium (A) for $x < L$ and another porous medium (B) for $x > L$, and return to the dimensional variables for a moment. These porous media have permeabilities K_A and K_B and thermal conductivities k_{mA} and k_{mB} , respectively. The dynamic condition combined with Darcy's law gives

$$\frac{1}{K_A} \frac{\partial \psi_A}{\partial x} = \frac{1}{K_B} \frac{\partial \psi_B}{\partial x}, \quad x = L.$$

We take the limit $K_A/K_B \rightarrow 0$ which is the correct description if the porous medium ends at $x=L$ and there is pure fluid for $x > L$. The result is

$$v = \frac{\partial \psi}{\partial x} = 0, \quad x = L$$

valid in medium (A), which confirms condition (11).

The dimensional heat equation for two-dimensional convection in a porous medium is¹⁵

$$\frac{(\rho c_p)_m}{(\rho c_p)_f} \frac{\partial \theta}{\partial t} - v \frac{\Delta T}{H} + u \frac{\partial \theta}{\partial x} + v \frac{\partial \theta}{\partial y} = \kappa_m \nabla^2 \theta.$$

The second term vanishes at the boundary $x=L$ because $v=0$ there. We consider linearized theory, which implies that the third and fourth terms are neglected everywhere in the fluid. The remaining equation is

$$\frac{(\rho c_p)_m}{(\rho c_p)_f} \frac{\partial \theta}{\partial t} = \kappa_m \nabla^2 \theta$$

valid in both media (A) and (B), at their common interface $x=L$. However, this is the equation of thermal conduction in a solid medium, without influence of the fluid flow. Conservation of energy is then expressed directly by Fourier law as a condition of continuity in conductive heat flux,

$$k_{mA} \frac{\partial \theta_A}{\partial x} = k_{mB} \frac{\partial \theta_B}{\partial x}, \quad x = L.$$

This condition is independent of time since the interface does not have any heat capacity. Here we see how the thermal condition (11) arises in the limit of great conductivity contrast between medium (A) and medium (B). The required conductivity limit $k_{mA} \gg k_{mB}$ is very well approximated if the solid is a metal and the saturating fluid is nonmetallic. From the Science Data Book¹⁶ we find typical conductivities of metals ranging from lead at 35 SI units ($\text{W m}^{-1} \text{K}^{-1}$) to copper at 385 SI units. This is indeed much greater than the typical values of thermal conductivities for nonmetallic liquids, ranging from turpentine at 0.136 SI units to water at 0.591 SI units. Most gases have still smaller conductivities, as the value for air at standard atmospheric pressure and temperature is only 0.024 SI units. For $x < L$ the effective conductivity of this mixture of metal solid and nonmetallic fluid will be of the same order of magnitude as the metal solid, provided the porosity of the porous medium is small enough for Darcy's law to be valid (neglecting the Brinkman correction terms and thereby excluding high-porosity media).

Now we have shown how a confined porous medium made of metal with moderate porosity and saturated with a nonmetallic fluid will approximate very well the condition

(11) of an open boundary where the porous medium leads into a hydrostatic reservoir for its saturating fluid. At $x=L$ the fluid mass will flow freely in and out from the porous medium, while heat transfer through this boundary will be effectively impeded.

Another possibility of satisfying condition (11) is to have a porous medium made of nonmetallic solid (e.g., polystyrene) for $x > L$. It will have much smaller conductivity than the metal medium. In order to have much greater permeability than the metal medium, the grain size of the nonmetallic solid must be much more coarsely grained than the metal medium.

From now on we again work with dimensionless variables. Equations (7) and (8) may be simplified by setting both ψ and θ to be proportional to $\sin \pi y$, since we may introduce such a Fourier decomposition in the vertical direction, and to $\exp(i\omega t)$, in order to allow the possibility of a Hopf bifurcation at neutral stability. Therefore we substitute

$$\psi = f(x) \sin(\pi y) e^{i\omega t}, \quad \theta = g(x) \sin(\pi y) e^{i\omega t}, \quad (12)$$

and so f and g satisfy the equations,

$$f'' - \pi^2 f = Rg', \quad g'' - \pi^2 g = -f' + i\omega g, \quad (13)$$

and are subject to

$$f(0) = g(0) = 0, \quad f'(a) = g'(a) = 0. \quad (14)$$

From a historical point of view it is worth noting at this stage that the substitution (12) is somewhat unusual in the context of Bénard convection since the Fourier decomposition takes place in the vertical direction, rather than in the horizontal direction. Similar substitutions have been used in the papers by Nilsen and Storesletten,¹² Rees and Lage,¹³ and Rees and Tyvand,¹⁴ but these papers share with the present paper the fact that the boundary conditions on each vertical surface are identical for both ψ and θ . The ramification of this is that the horizontal component of the eigenfunctions at onset are not pure sines or cosines, but are more complicated functions.

III. NUMERICAL SOLUTIONS

Equations (13) subject to (14) were solved using the classical fourth-order Runge–Kutta scheme with the shooting method. The equations were decomposed into real and imaginary parts with $f = f_r + if_i$ and $g = g_r + ig_i$, and two extra first-order equations defined as

$$R' = 0, \quad \omega' = 0. \quad (15)$$

The boundary conditions given in (14) were supplemented by the normalization conditions

$$g'_r(0) = 1, \quad g'_i(0) = 0. \quad (16)$$

Thus the full system is now of tenth order with a total of 10 boundary conditions.

The only free parameter is the aspect ratio of the cavity and this was varied between 0.02 and 20. Figures 1 and 2 show how the critical Rayleigh number and the angular frequency vary with the cavity aspect ratio. The critical Rayleigh number decreases towards $4\pi^2$ as a increases, but in-

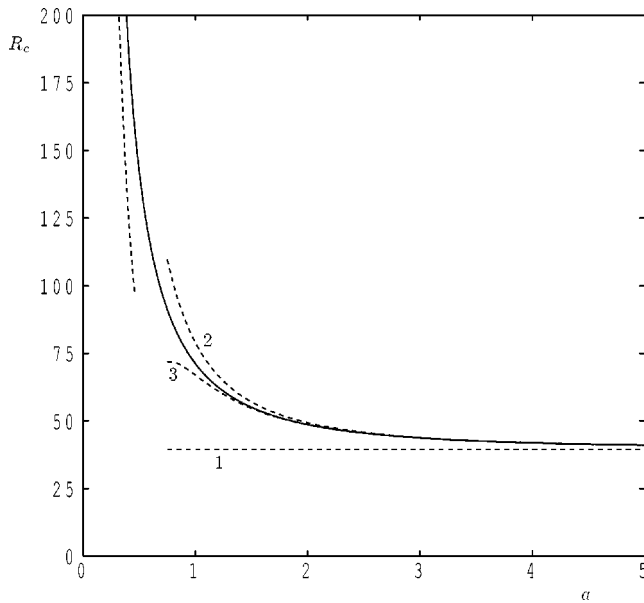


FIG. 1. Critical Rayleigh number as a function of aspect ratio a . Also shown as dashed curves are the small- a asymptotic curve and the 1-term, 2-term, and 3-term large- a asymptotic curves (labeled 1, 2, and 3, respectively).

creases substantially as $a \rightarrow 0$. The value of $4\pi^2$ corresponds to the classical Lapwood–Horton–Rogers stability criterion in an unbounded horizontal layer, and therefore the vertical boundaries have a diminishing effect as the cavity increases in horizontal extent. A detailed analysis of the values of R_c , some of which are given in Table I, indicates that they satisfy $R_c = 4\pi^2 + O(a^{-2})$ when $a \gg 1$ and $R_c = O(a^{-2})$ when $a \ll 1$; both of these trends are confirmed and quantified in the following section. As in Ref. 14 the variation of R_c is smooth and monotonic, unlike the situation where the sidewalls are impermeable and insulated (see Refs. 10 and 17) where R_c displays an infinite series of minima at $R = 4\pi^2$ between which the number of cells increases suddenly by 1.

In all cases the wave speed of the convection cells is positive and, like R_c , it is a monotonically decreasing function of a . The detailed values of ω indicate that $\omega = O(a^{-3})$ when $a \gg 1$ and $\omega = O(a^{-2})$ when $a \ll 1$.

Figure 3 shows the computed variation of f and g with x for four choices of cavity aspect ratio: $a = 1, a = 2, a = 5,$ and $a = 20$. In all cases the real and imaginary parts of f have

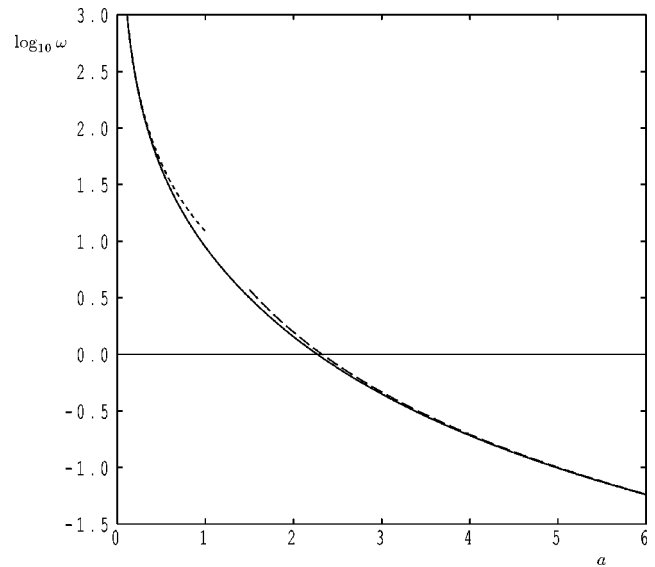


FIG. 2. Critical angular frequency ω as a function of aspect ratio a . Also shown as dashed lines are the 1-term asymptotic curves for both small and large values of a .

zeros which interleave—these correspond to the locations of cell walls at different times, namely, when ωt is a multiple of π and when it is $\pi/2$ greater than a multiple of π , respectively. Thus the cells move in the positive x direction.

As a increases it is evident that two spatial scales dominate. One is roughly of unit length while the other is comparable with the length of the cavity. This observation forms the basis for the large- a asymptotic analysis found in the following section. However, we note that the solution given in Fig. 3(d) is almost identical to that given by Rees and Tyvand where the sidewalls are both conducting and impermeable. In the present case there is a slight adjustment in the solution near $x = a$ in order to satisfy the zero derivative boundary conditions.

Figure 4 shows streamlines and perturbation isotherms at equally spaced time intervals over a quarter of a period for convection in a box of aspect ratio $a = 3$. The continuous lines represent streamlines and the dashed lines perturbation isotherms, but they may also be taken the other way around. The precise location of the streamlines in the first frame of Fig. 4 is identical to the isotherms in the last frame. This

TABLE I. Variation of R_c and ω with a . Also shown are suitable asymptotic values for the limits $a \rightarrow 0$ and $a \rightarrow \infty$.

a	R_c	$R_c a^2$	$(R_c - 4\pi^2)a^2$	ω	ωa^2	ωa^3
0.0		20.5344			12.1875	
0.1	2120.7916	21.2079		1212.607 1	12.1261	
0.2	579.5466	23.1819		298.711 1	11.9484	
0.5	142.1563	35.5391		43.715 1	10.9288	
1	71.1982	71.1982	31.7198	8.871 0	8.8710	8.8710
2	48.6690		36.7623	1.431 2		11.4496
5	41.0387		39.0075	0.099 05		12.3813
10	39.8720		39.36	0.012 52		12.52
∞			39.4784			12.5664

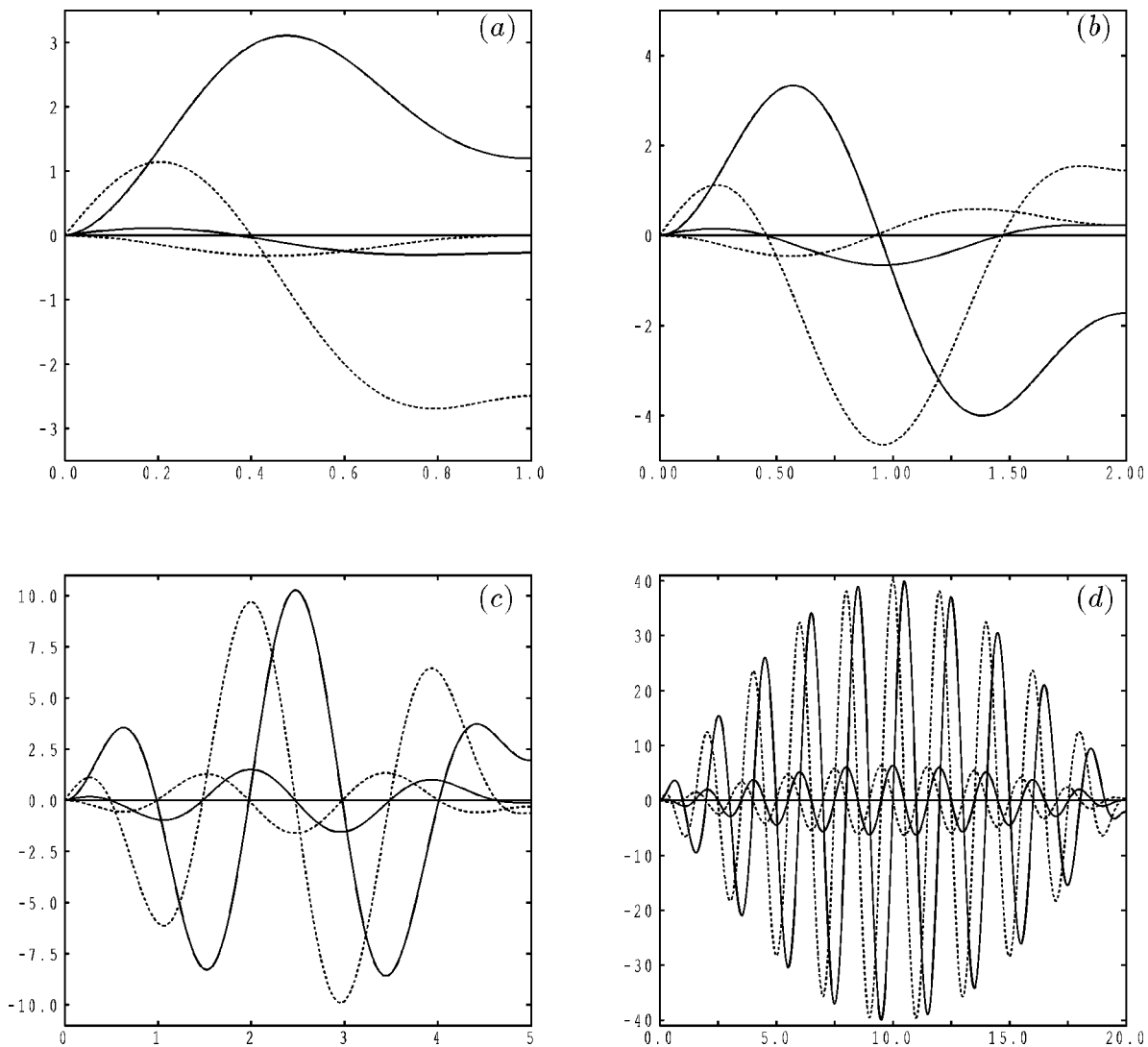


FIG. 3. Real and imaginary parts of f and g forming solutions of Eqs. (13) and (14). In each part continuous lines correspond to the real part of the solution while the dashed lines correspond to the imaginary part. The two curves with the largest amplitudes correspond to $\text{Re}(f)$ and $\text{Im}(f)$. The parts are for domains with (a) $a=1$; (b) $a=2$; (c) $a=5$; (d) $a=20$.

figure shows clearly the manner in which the convecting cells travel towards the open insulated boundary. Although the value of ω is constant, the fact that the zeros in, say, f_r and f_i are not equally spaced means that cell walls do not travel at a uniform speed towards the right-hand sidewall. That this is so may be seen in the first four frames of Fig. 4 where the right-hand vertical streamline accelerates towards the right-hand boundary. Likewise we see that the length of the cells is not uniform but varies over time and with x : while the central cell in the last frame of Fig. 4 has aspect ratio of almost exactly 1, the right-hand cell is stretched horizontally so that both ψ and θ satisfy Neumann conditions.

IV. ASYMPTOTIC ANALYSIS

In this section we supplement the above numerical results by undertaking analyses in limits of both small and large aspect ratios.

A. Small aspect ratios

When the aspect ratio is small the numerical solutions indicate that both R and ω are of $O(a^{-2})$. Given that $g'(0) = 1$ is the normalizing condition and that $x = O(a)$ within the cavity, it is straightforward to show that $g = O(a)$. An order of magnitude analysis confirms the above statements regarding the sizes of R and ω , and we also find that $f = O(1)$. We may now rescale according to

$$x = \xi a, \quad R = S/a^2, \quad \omega = \Omega/a^2, \quad f(x) = F(\xi), \quad g(x) = aG(\xi). \tag{17}$$

Equations (13) become

$$F'' = SG', \quad G'' + F' = i\Omega G, \tag{18}$$

subject to

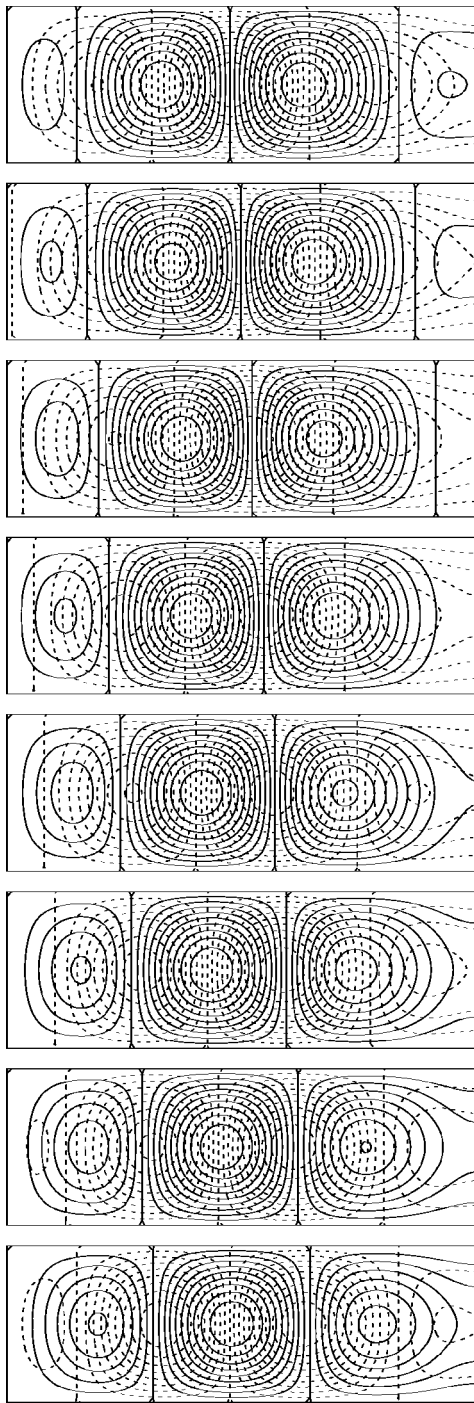


FIG. 4. Streamlines and isotherms at equally spaced time intervals over one-quarter of a period for convection in a cavity of aspect ratio $a=3$ at the critical Rayleigh number. Time increases downwards.

$$F(0) = G(0) = 0, \quad G'(0) = 1, \quad F'(1) = G'(1) = 0. \quad (19)$$

These equations were solved numerically using the same Runge–Kutta scheme to obtain the values

$$S = 20.5344, \quad \Omega = 12.1875, \quad (20)$$

and therefore we have

$$R \sim 20.5344/a^2, \quad \omega \sim 12.1875/a^2 \quad (21)$$

as $a \rightarrow 0$. Both these expressions compare very well indeed with the data given in Table I and displayed in Figs. 1 and 2. Clearly the angular frequency appears to increase without bound as the cavity becomes thinner, but we note that, should the Rayleigh number be based upon the width of the cavity, rather than on its height, then the Rayleigh number and the angular frequency would tend towards the respective constants given in (20).

B. Large aspect ratios

When the cavity has a large aspect ratio the eigensolutions display two very distinct length scales. One of these is commensurate with the length of the cavity and the other is roughly equal to 1. Thus the solution given in Fig. 3(d) for $a=20$ indicates that the solutions consist of the product of $e^{i\pi x}$ and $\sin(\pi x/a)$ at least to leading order. There is also a minor adjustment near to $x=a$ where the stream function and temperature fields, which are $\pi/2$ out of phase in the bulk of the cavity, are forced to obey the same boundary conditions. It is not entirely clear from Fig. 3(d) that the main cellular pattern has a wave number of precisely π , but any changes from this are likely to be asymptotically small when a is large, and therefore such small wave number changes are assumed to be accounted for using multiple scales theory.

The full equations for f and g are

$$f'' - \pi^2 f = Rg', \quad g'' - \pi^2 g = -f' + i\omega g, \quad (22)$$

subject to $f(0)=g(0)=0$, $g'(0)=\text{const}$ and $f'(a)=g'(a)=0$. We set $\epsilon=1/a$ as the asymptotically small parameter, and will assume that both f and g are proportional to $\exp(i\pi x)$. We therefore introduce the following substitutions:

$$f = 2\pi F(X)e^{i\pi x}, \quad g = iG(X)e^{i\pi x}, \quad (23)$$

where

$$X = \epsilon x, \quad \omega = \epsilon^2 \Omega, \quad R = 4\pi^2 S. \quad (24)$$

The solution proceeds in powers of ϵ and therefore we also introduce the expansions

$$F(X) = F_0(X) + \epsilon F_1(X) + \epsilon^2 F_2(X) + \dots, \quad (25)$$

$$G(X) = G_0(X) + \epsilon G_1(X) + \epsilon^2 G_2(X) + \dots, \quad (26)$$

and

$$S = S_0 + \epsilon S_1 \epsilon^2 S_2 + \dots. \quad (27)$$

All of the above expansions and substitutions transform Eqs. (22) into the following forms:

$$(S_0 + \epsilon S_1 + \epsilon^2 S_2 + \dots)G - F + \left(\frac{i\epsilon}{\pi}\right)F_X - \left(\frac{i\epsilon}{\pi}\right)G_X(1 + \epsilon S_1 + \epsilon^2 S_2 + \dots) + \left(\frac{\epsilon^2}{2\pi^2}\right)F_{XX} = 0 \quad (28)$$

and

$$(F - G) + \frac{i\epsilon}{\pi}(G_X - F_X) + \frac{\epsilon^2}{2\pi^2}G_{XX} + \frac{\epsilon^2 i \Omega}{2\pi^2}G = 0. \quad (29)$$

At $O(1)$ we obtain

$$S_0 G_0 - F_0 = 0, \quad F_0 - G_0 = 0, \quad (30)$$

from which we deduce that

$$S_0 = 1, \quad F_0 = G_0 = A(X), \quad (31)$$

where $A(X)$ is to be obtained below at $O(\epsilon^2)$. Given the boundary conditions for f and g at $x=0$ it is essential that $A(0)=0$. At $x=a$, however, both f_x and g_x , which are proportional to $[i\pi A(X) + \epsilon A_X(X)]e^{i\pi x}$, must have zero derivatives. This means that the second boundary condition for A is $A(1)=0$; the $O(\epsilon)$ term is accounted for at higher order.

At $O(\epsilon)$ Eqs. (28) and (29) yield

$$G_1 - F_1 = -S_1 G_0, \quad F_1 - G_1 = 0. \quad (32)$$

A simple solvability condition for this pair of equations is obtained by adding them together, in which case we obtain

$$S_1 = 0, \quad F_1 = G_1 = B(X), \quad (33)$$

where $B(X)$ is found at $O(\epsilon^3)$.

At $O(\epsilon^2)$ we have

$$G_2 - F_2 = -S_2 G_0 - \frac{1}{2\pi^2} F_{0XX}, \quad F_2 - G_2 = -\frac{1}{2\pi^2} G_{0XX}, \quad (34)$$

which, after addition and substitution using (30), yields the solvability condition

$$A_{XX} + \pi^2 S_2 A_0 = 0. \quad (35)$$

Above we derived the boundary conditions, $A(0)=A(1)=0$, and therefore the smallest possible value of S_2 which yields a nonzero solution is $S_2=1$ and therefore we have

$$A(X) = \sin \pi X. \quad (36)$$

Equations (34) may now be solved:

$$F_2(X) = C(X) + \frac{1}{2} \sin \pi X, \quad G_2(X) = C(X), \quad (37)$$

where $C(X)$ is an unknown function of X . Thus far in the analysis we have $R \sim 4\pi^2(1+1/a^2)$ which is not only correct to $O(\epsilon^2)$ but is identical to the value of R obtained by Rees and Tyvand¹⁴ for the cavity with a fully impermeable and conducting boundary. It is at the next order that the first difference is found between their solutions and the present solutions.

At $O(\epsilon^3)$ the equations become

$$G_3 - F_3 = -S_3 G_0 - S_2 G_1 - \frac{i}{\pi} F_{2X} + \frac{i}{\pi} (G_{2X} + S_2 G_{0X}) - \frac{1}{2\pi^2} F_{1XX}, \quad (38a)$$

$$F_3 - G_3 = -\frac{i}{\pi} (G_{2X} - F_{2X}) - \frac{1}{2\pi^2} G_{1XX} - \frac{i\Omega}{2\pi^2} G_0. \quad (38b)$$

Substitution for G_0 , F_1 , G_1 , F_2 , and G_2 , and addition of the two equations eventually yield

$$B_{XX} + \pi^2 B = -\pi^2 S_3 \sin \pi X + i\pi^2 \cos \pi X - \frac{i\Omega}{2} \sin \pi X. \quad (39)$$

The function B also satisfies a zero boundary condition at $X=0$, but the condition at $X=1$ requires more care. On writing $g(x)$ to $O(\epsilon)$ we have $g=i[A(X)+\epsilon B(X)]e^{i\pi x}$, and therefore dg/dx at $x=a$ is

$$\frac{\partial g}{\partial x}(a) = i\{i\pi A(1) + \epsilon[A_X(1) + i\pi B(1)] + \dots\}e^{i\pi\delta}, \quad (40)$$

where we have set $a=2N+\delta$ as the length of the cavity, and where $N \gg 1$ and $0 \leq \delta < 2$. The $O(\epsilon)$ term in (40) must be zero and therefore

$$B(1) = -i. \quad (41)$$

The full solution of (39) is

$$B = \frac{i\pi}{2} X \sin \pi X + \left(\frac{\pi}{2} S_3 + \frac{i}{4\pi} \Omega \right) X \cos \pi X + c \sin \pi X, \quad (42)$$

where c is an arbitrary constant. But (41) must be satisfied and therefore

$$\left(\frac{\pi}{2} S_3 + \frac{i}{4\pi} \Omega \right) = i, \quad (43)$$

from which we obtain

$$S_3 = 0, \quad \Omega = 4\pi. \quad (44)$$

The wave speed of the cells is, therefore,

$$\omega \sim 4\pi/a^3, \quad (45)$$

which also accords very well with the data given in Table I and Fig. 2.

We omit details of the analysis at $O(\epsilon^4)$ but the solvability condition yields $S_4 = -3/\pi^2$ but no correction to the wave speed. Therefore the critical Rayleigh number is

$$R \sim 4\pi^2 \left[1 + \frac{1}{a^2} - \frac{3}{\pi^2 a^4} \right]. \quad (46)$$

The first two terms of this expression are graphically indistinguishable from the exact solution when $a > 3$ as opposed to $a > 2$ for all three terms. In fact, (46) has a relative error of slightly more than 10^{-4} even when a is as small as 3.

V. CONCLUSIONS

In this paper we have performed a linearized stability analysis of the onset of convection in a porous cavity which exhibits what we term nontraditional boundary conditions: The left-hand boundary is impermeable and thermally conducting, while the right-hand boundary is open and thermally insulating. In an earlier paper (Rees and Tyvand¹⁴) we studied convection in a cavity with the first type of nontraditional condition (impermeable and conducting) assumed valid everywhere. This had the effect of causing degeneracy in the onset problem, first demonstrated by Lyubimov.¹⁸ Moreover, convection may take place with any phase relative to the

location of the sidewalls. In the present problem the cavity is asymmetric with respect to the sidewall boundary conditions. This causes the onset problem to be of Hopf type with cells traveling towards the open, insulated sidewall.

Detailed numerical solutions have been presented and supplemented by separate asymptotic analyses valid for small and large cavity aspect ratios. It was found that both the critical Rayleigh number and angular frequency decrease monotonically as the aspect ratio increases.

Both this paper and the preceding one, Rees and Tyvand,¹⁶ are concerned with the effect of nontraditional boundary conditions on two-dimensional convection. At present it is not clear whether the findings of these papers, in particular degeneracy and time-dependent onset, carry over to three-dimensional cavities. The only hint of which we are aware is the analysis of Storesletten and Tveitereid¹⁹ on convection in a horizontal cylinder where the critical Rayleigh numbers corresponding to the first two modes of instability tend to a common limit as the axial wave number tends to zero. Thus the degeneracy noted by Rees and Tyvand¹⁴ is recovered. Work is currently in progress to investigate both this aspect and the effects of strongly nonlinear postcritical convection.

The present work adds to the developing understanding of the Rayleigh–Bénard problem for a two-dimensional porous box, starting with the work by Beck.¹⁰ He restricted himself to the traditional conditions of insulating sidewalls and conducting top and bottom, with all walls impermeable. Let us define a traditional condition as one allowing a single Fourier eigenmode for the temperature and stream function. Accordingly, these are the possible traditional conditions:

Traditional conditions at top and bottom:

- (I) conducting and impermeable,
- (II) insulating (heat flux given) and open (constant pressure).

Traditional conditions at sidewalls:

- (a) insulating and impermeable,
- (b) conducting and open.

All these conditions are idealized in the sense that the boundary is either completely closed or completely open with respect to throughflow of heat and mass. The remaining possibilities are the nontraditional conditions:

Nontraditional conditions at top and bottom:

- (III) Insulating (heat flux given) and impermeable,
- (IV) conducting and open (constant pressure).

Nontraditional conditions at sidewalls:

- (c) Conducting and impermeable,
- (d) insulating and open.

A striking fact is that the two conditions that are traditional at the top and bottom appear as nontraditional when applied on the sidewalls, and vice versa. So far, no solution exists for the Rayleigh–Bénard problem with nontraditional

conditions applied at horizontal as well as vertical boundaries. Nield³ solved the problem with all varieties of conditions (I)–(IV) at top and bottom, but he implicitly assumed traditional lateral conditions as he considered infinite horizontal extent. Nield and Bejan²⁰ (Table 6.1, page 147) has given a systematic overview of these conditions (I)–(IV) applied at the top and bottom, counting 10 nontrivial combinations. Tyvand²¹ (Table 4.1, page 94) has given a similar overview of all varieties of the conditions (a)–(d) applied at the lateral walls, again identifying ten nontrivial combinations. The present problem appeared in this table as the only unsolved case. Again the simplest traditional condition (I) was applied at the other boundaries (top and bottom).

The present work completes the picture of all possible idealized conditions (a)–(d) at lateral walls,²¹ as a counterpart to all possible idealized conditions at top and bottom.²⁰ Furthermore, we open up a variety of some solved and many unsolved two-dimensional Rayleigh–Bénard problems: A 10×10 matrix of eigenvalue problems arises from the 10 nontrivial combinations of top and bottom conditions taken together with the 10 nontrivial combinations of left-hand and right-hand wall conditions. The published tables^{20,21} comprise 19 out of these 100 eigenvalue problems ($19 = 10 + 10 - 1$ since there is one overlapping case). Some of the remaining 81 cases are straightforward to deduce from the tables of results,^{20,21} yet no results are known for any eigenvalue problem with nontraditional conditions being posed at the horizontal as well as the vertical boundaries. The common mathematical difficulty for such eigenvalue problems is that they are not separable in the x and y directions, and it will not be straightforward to find any closed-form analytical solutions.

APPENDIX: A PROOF THAT THERE ARE NO STEADY EIGENSOLUTIONS

We consider the steady-state version of the governing equations. We introduce a modified complex stream function Ψ by the definition

$$\psi = i\sqrt{R}\Psi. \tag{A1}$$

The resulting coupled equations for θ and Ψ are

$$\nabla^2\Psi + i\sqrt{R}\frac{\partial\theta}{\partial x} = 0, \tag{A2}$$

$$\nabla^2\theta + i\sqrt{R}\frac{\partial\Psi}{\partial x} = 0, \tag{A3}$$

where the conditions

$$\Psi = \theta = 0 \text{ along the boundary} \tag{A4}$$

correspond to impermeable and conducting boundaries, valid along the bottom ($y=0$) and top ($y=1$) as well as the left-hand wall ($x=0$). Along the right-hand wall we have the conditions

$$\frac{\partial\Psi}{\partial x} = \frac{\partial\theta}{\partial x} = 0 \text{ at } x = a. \tag{A5}$$

We conclude that the coupled eigenvalue problem is completely symmetric in Ψ and θ . If we eliminate θ to formulate

the eigenvalue problem in terms of Ψ alone, then this will be identical to the problem written in terms of θ which we get by eliminating Ψ . This complete symmetry in Ψ and θ implies that the solutions must be the same, i.e.,

$$\Psi(x, y) = \theta(x, y), \quad (\text{A6})$$

provided that there is a unique solution of this complex eigenvalue problem given by (A2)–(A5).

Inserting Eq. (A6) into the second governing Eq. (A3) reduces the problem from a fourth-order problem to a second-order problem,

$$\nabla^2 \theta + i\sqrt{R} \frac{\partial \theta}{\partial x} = 0, \quad (\text{A7})$$

with the boundary conditions

$$\theta = 0 \quad \text{at} \quad y = 0, \quad y = 1, \quad x = 0, \quad (\text{A8})$$

$$\frac{\partial \theta}{\partial x} = 0, \quad x = a. \quad (\text{A9})$$

As in the main text, we separate out the vertical dependence: $\theta = g(x) \sin(\pi y)$. The eigenfunction $g(x)$ is governed by the boundary value problem

$$g'' + i\sqrt{R}g' - \pi^2 g = 0, \quad (\text{A10})$$

$$g(0) = g'(a) = 0. \quad (\text{A11})$$

The general solution is

$$g = A \exp\left(\frac{i}{2}R_1 x\right) + B \exp\left(\frac{i}{2}R_2 x\right), \quad (\text{A12})$$

where we have introduced $R_1 = -\sqrt{R} + \sqrt{R - 4\pi^2}$ and $R_2 = -\sqrt{R} - \sqrt{R - 4\pi^2}$. This is the correct solution provided $R_1 \neq R_2$ so that there are two linearly independent eigenfunctions. The left-hand boundary condition at $x=0$ gives $B = -A$, so that we may write

$$g = C \exp\left(-\frac{i\sqrt{R}x}{2}\right) \sin\left(x \sqrt{\frac{R}{4} - \pi^2}\right),$$

where C is a redefined amplitude. The right-hand boundary condition at $x=a$ gives the complex equation

$$C \left[i\sqrt{R} \sin\left(a \sqrt{\frac{R}{4} - \pi^2}\right) + \sqrt{R - 4\pi^2} \cos\left(a \sqrt{\frac{R}{4} - \pi^2}\right) \right] = 0. \quad (\text{A13})$$

There are two possibilities of satisfying the right-hand boundary condition: The first option is the trivial solution $C=0$. The second option is the relationship $R=4\pi^2$, which is the only nontrivial way of satisfying both the real and imagi-

nary parts of Eq. (A13). However, this value of R makes the eigenfunctions linearly dependent because $R_1=R_2$. For this value of R , the characteristic equation has a double root, and the correct solution will be

$$g(x) = (A + Bx)e^{i\pi x}. \quad (\text{A14})$$

The condition $g(0)=0$ implies $A=0$, and the condition $g'(a)=0$ implies $B=0$. Then the eigenfunction (A14) becomes zero, which means that nontrivial eigenfunctions do not exist. We have thus proven that there are no steady-state solutions of the eigenvalue problem. This means that oscillatory modes of convection are the only possible solutions.

¹C. W. Horton and F. T. Rogers, "Convection currents in a porous medium," *J. Appl. Phys.* **16**, 367 (1945).

²E. R. Lapwood, "Convection of a fluid in a porous medium," *Proc. Cambridge Philos. Soc.* **44**, 508 (1948).

³D. A. Nield, "Onset of thermohaline convection in a porous medium," *Water Resour. Res.* **11**, 553 (1968).

⁴J. M. Straus, "Large amplitude convection in porous media," *J. Fluid Mech.* **64**, 51 (1974).

⁵R. N. Horne and M. J. O'Sullivan, "Oscillatory convection in a porous medium heated from below," *J. Fluid Mech.* **66**, 339 (1974).

⁶C. K. Aidun and P. H. Steen, "Transition to oscillatory heat transfer in a fluid-saturated porous medium," *Int. J. Thermophys.* **1**, 268 (1987).

⁷S. Kimura, G. Schubert, and J. M. Straus, "Instabilities of steady, periodic and quasi-periodic modes of convection in porous media," *Trans. ASME, Ser. C: J. Heat Transfer* **109**, 350 (1987).

⁸S. Kimura, G. Schubert, and J. M. Straus, "Time-dependent convection in a fluid-saturated porous cube heated from below," *J. Fluid Mech.* **207**, 153 (1987).

⁹R. A. Wooding, "Steady state free thermal convection of liquid in a saturated permeable medium," *J. Fluid Mech.* **2**, 273 (1957).

¹⁰J. L. Beck, "Convection in a box of porous material saturated with fluid," *Phys. Fluids* **15**, 1377 (1972).

¹¹A. Zebib, "Onset of natural convection in a cylinder of water-saturated porous media," *Phys. Fluids* **21**, 699 (1978).

¹²T. Nilsen and L. Storesletten, "An analytical study on natural-convection in isotropic and anisotropic porous channels," *ASME Trans. J. Heat Transfer* **112**, 396 (1990).

¹³D. A. S. Rees and J. L. Lage, "The effect of thermal stratification on natural convection in a vertical porous insulation layer," *Int. J. Heat Mass Transfer* **40**, 111 (1997).

¹⁴D. A. S. Rees and P. A. Tyvand, "The Helmholtz equation for convection in two-dimensional porous cavities with conducting boundaries," *J. Eng. Math.* **49**, 181 (2004).

¹⁵Y. Katto and T. Masuoka, "Criterion for the onset of convective flow in a fluid in a porous medium," *Int. J. Heat Mass Transfer* **10**, 297 (1967).

¹⁶R. M. Tennent, *Science Data Book* (Oliver & Boyd, Edinburgh, 1971), pp. 60–63.

¹⁷C. K. Aidun, "Stability of convection rolls in porous media," *Proceedings of the ASME Winter Annual Meeting*, Boston, 1987.

¹⁸D. V. Lyubimov, "Convective motions in a porous medium heated from below," *J. Appl. Mech. Tech. Phys.* **16**, 257 (1975).

¹⁹L. Storesletten and M. Tveitereid, "Natural convection in a horizontal porous cylinder," *Int. J. Heat Mass Transfer* **34**, 1959 (1991).

²⁰D. A. Nield and A. Bejan, *Convection in Porous Media*, 2nd ed. (Springer, New York, 1999).

²¹P. A. Tyvand, in *Transport Phenomena in Porous Media II*, edited by D. B. Ingham and I. Pop (Pergamon, London, 2002), pp. 82–112.